Computers and Concrete, *Vol. 24, No. 5 (2019) 423-436*
DOI: https://doi.org/10.12989/cac.2019.24.5.423

Design equation to evaluate bursting forces at the end zone of post-tensioned members

Joung Rae Kim[1a], Hyo-Gyoung Kwak[*1] and Byung-Suk Kim[2]

[1]Department of Civil and Environmental Engineering, Korea Advanced Institute of Science and Technology (KAIST), Daejeon 34141, Republic of Korea
[2]Korea Institute of Civil Engineering and Building Technology, Republic of Korea

(*Received January 20, 2019, Revised September 25, 2019, Accepted October 5, 2019*)

Abstract. Design equations to evaluate the bursting force in a post-tensioned anchorage zone have been introduced in many design codes, and one equation in AASHTO LRFD is widely used. However, this equation may not determine the bursting force exactly because it was designed on the basis of two-dimensional numerical analyses without considering various design parameters such as the duct hole and shape of the bearing plate. To improve the design equation, modification of the AASHTO LRFD design equation was considered. The behavior of the anchorage zone was investigated using three-dimensional linear elastic finite element analysis with design parameters such as bearing plate size and diameter of sheath hole. Upon the suggestion of a modified design equation for evaluating the bursting force in an anchorage block with a rectangular anchorage plate (Kim and Kwak 2018), additional influences of design parameters that could affect the evaluation of bursting force were investigated. An improved equation was introduced for determining the bursting force in an anchorage block with a circular anchorage plate, using the same procedure introduced in the design equation for an anchorage block with a rectangular anchorage plate. The validity of the introduced design equation was confirmed by comparison with AASHTO LRFD.

Keywords: bursting force; anchorage zone; duct hole; multiple anchorage; circular bearing plate

1. Introduction

In post-tensioned prestressed concrete structures with mechanical anchorages, the tendons are stressed and anchored at the ends of the concrete members, and the prestressing force is essentially transferred from the tendons to the concrete by the anchorage bearing plates. The end zone of each concrete member is then subjected to a transition of compressive stress from concentrated to linearly distributed over the cross section (Guyon 1953). This transition of longitudinal compressive stress produces transverse tensile stresses that may lead to longitudinal bursting cracks in the member. The pattern and magnitude of the concrete stresses depend on the location and distribution of the concentrated forces applied by the tendons.

These tensile stresses must be determined with some degree of accuracy so that the concrete, which by itself has a low tensile strength, can be adequately reinforced to resist them (Fenwick and Lee 1986). The bursting stress distribution in the end zone has been analyzed using the methods of classical elasticity, photoelasticity, and finite element (FE) analysis (Guyon 1953, Saadoun 1980, Burdet 1990). In addition, elastic analysis, which offers larger stress distribution than plastic analysis, has been traditionally used because any structural design must meet safety requirements (Adeghe and Collins 1986, Fenwick and Lee 1986). To understand the stress distribution in an anchorage zone and effectively place reinforcements, a lot of research has been undertaken to evaluate the bursting tensile force (Guyon 1953, Burdet 1990, He and Liu 2011). Such studies have been based on a number of mechanical concepts, including the theory of elasticity, FE analysis, the strut-and-tie method, as well as other experimental approaches. Comprehensive reviews of previous studies can be found elsewhere (Breen *et al*. 1994, Rogowsky and Marti 1996, Songwut 2004, Callaghan and Bayrak 2008, Zhou *et al*. 2015).

The results obtained from many experimental and numerical studies have subsequently been implemented in design codes (Schlaich *et al*. 1987, Burdet 1990, Wollman 1992, Sanders and Breen 1997). One design formula for the anchorage zone, introduced following extensive FE analysis by Burdet (1990), is mentioned in the AASHTO LRFD design guidelines (AASHTO LRFD 2012) and is widely used as part of the design process. Nevertheless, this design formula does not have an adequate theoretical basis for considering many design parameters because it was primarily developed using two-dimensional (2D) FE analysis. For example, it does not consider the duct hole, which causes stress concentration. To improve this equation, Kim and Kwak (2018) recently suggested an improved formula to evaluate the bursting force in an anchorage block with a rectangular bearing plate. The suggested formula considered the contribution of the duct

*Corresponding author, Professor
E-mail: kwakhg@kaist.ac.kr
[a]Ph.D. Candidate
E-mail: tootooi3@kaist.ac.kr

http://www.techno-press.org/?journal=cac&subpage=8
ISSN: 1598-8198 (Print), 1598-818X (Online)

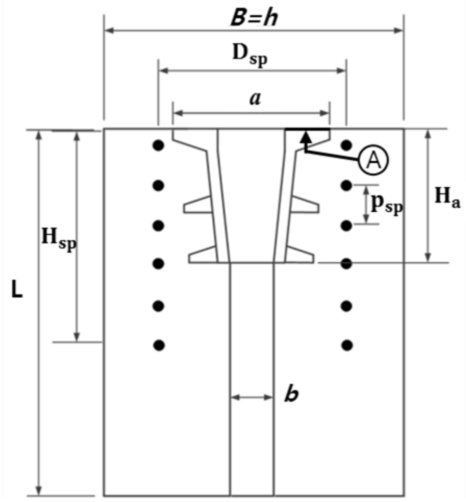

Fig. 1. Apparatus for the load transfer test
L=length of specimen, $B=h$=width of specimen, a=diameter of bearing plate, H_a=height of anchorage device, b= diameter of duct hole, D_{sp}=diameter of spiral, d_{sp}=diameter of spiral, p_{sp}=pitch of spiral, H_{sp}=height of spiral

hole, and its efficiency was verified by three-dimensional (3D) FE analysis. This formula considered the influencing factors of the bearing plate size, eccentricity, and the tendon inclination.

Nevertheless, additional influencing factors that may affect the bursting tensile force need to be examined. Among them, the use of multiple anchorage blocks, the placement of a spiral reinforcement, and consideration of the trumpet imbedded in the concrete matrix may cause a change in the bursting force. These influences on the bursting tensile force need to be analyzed.

Based on this background, we investigated a number of parametric studies evaluating the relative effect of these design components on the bursting tensile force in an anchorage block through 3D FE analysis using ABAQUS (Dassault Systèmes 2013). In addition, the increase in bursting tensile stresses when a circular anchorage plate is used was also studied. Another design formula is then newly suggested for evaluating the bursting force in an anchorage block with a circular anchorage plate based on the same procedure employed by Kim and Kwak (2018) for a rectangular anchorage plate.

2. FE Idealization and its experimental verification

Since the numerical analyses conducted in our study are based on linear elastic analysis, the stress-strain relations of concrete and steel do not need to be defined. Only the modulus of elasticity and Poisson's ratio for concrete and steel are required. The elastic modulus of concrete and steel is defined according to the formulas $E_c = 8{,}500\sqrt[3]{f_c'} = 28{,}000\text{MPa}$ and $E_s = 210\text{GPa}$ in the Korea Concrete Institute (KCI) design code (2009), which is equivalent to the American Concrete Institute (ACI) design code (2014), and for the Poisson's ratio of concrete and steel, values of $\nu_c = 0.18$ and $\nu_s = 0.33$ were considered.

Table 1 Dimensions of anchorage zone specimens (mm)

Specimen	L	$B=h$	a	H_a	b	D_{sp}	d_{sp}	p_{sp}	No. of spirals	H_{sp}
1	720	360	250	200	114	298	16	50	7	350
2	1100	550	390	312	174	480	19	50	11	550

The accuracy of the numerical modeling of the anchorage block was verified in advance through correlation studies between the experimental data and the numerical results. Two load transfer test specimens tested at Research Institute of Science and Technology (RIST) (Kwon *et al*. 2015), Specimens 1 and 2, were selected, and Fig. 1 and Table 1 show the detailed dimensions of the anchorage zone components. As shown in Fig. 1 and Table 1, the test specimens are composed of three parts, a concrete matrix, an anchorage device, and spiral reinforcement, and utilize a circular bearing plate with diameter a. When the specimen is assembled, the three constituent parts of the anchorage zone must be in constant contact with each other. Thus, a perfect bond was applied in the numerical modeling of the specimens.

Because of the structural symmetry, only a quarter portion of the specimen was represented in the numerical modeling by ABAQUS. The bottom surface had no displacement along the longitudinal axis, and the two vertical side surfaces were set to satisfy the symmetric condition. In advance, no rotation for these two surfaces was allowed.

In our study, 3D solid elements (named C3D20R element in ABAQUS) were used in the numerical modeling of the concrete matrix, anchorage device, and spiral confinement reinforcement (see Fig. 2). Different from the ultimate strength of anchorage zone which the anchorage device leads to the higher resisting capacity (Marchão *et al*. 2019), an increase of bursting stress induced by a wedge effect does not appear in a real structural response accompanying the slip behavior along a trumpet surface (Burdet 1990). In this regard, the inclination of the trumpet was excluded in the numerical modeling as in AASHTO LRFD (2012). Moreover, to ensure consistency in the numerical modeling, the mesh size of each element was based on an equal length of 17 mm regardless of the differences in the sizes of the specimens. The dimensions of 17 mm×17 mm×17 mm were determined through the convergence test of the FE mesh size based on modeling the concrete matrix and the number of concrete elements. The same principle for numerical modeling was also applied to the other parts of the anchorage device and spiral reinforcement. On the basis of the symmetric shape of the anchorage zone, the anchorage zones were modeled over a quarter portion of the specimen and to deliver the confinement effect, spiral reinforcement was described with hoop reinforcement. Accordingly, the symmetric condition was applied on two vertical side surfaces. The bottom surface was fixed so that there was no displacement along the longitudinal axis. The loading process was guaranteed by controlling the displacement of the bearing plate. Since the bearing plate was sufficiently rigid, the application of

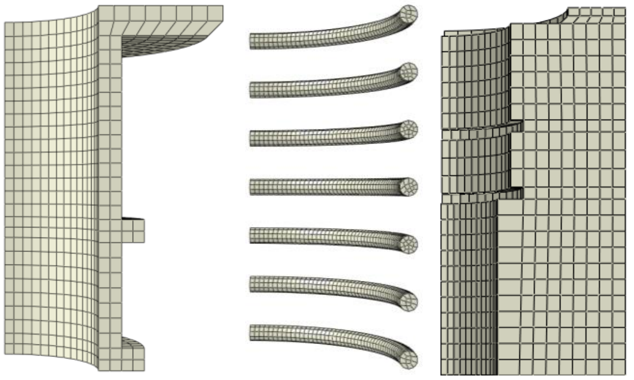

(a) anchorage device (b) spiral reinforcement (c) concrete matrix

Fig. 2 FE idealizations (90° revolved)

(a) before test (b) during test

Fig. 3 Representative features of test Specimen 2

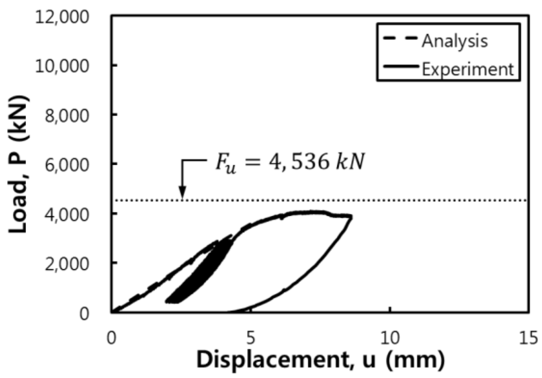

(a) Specimen 1

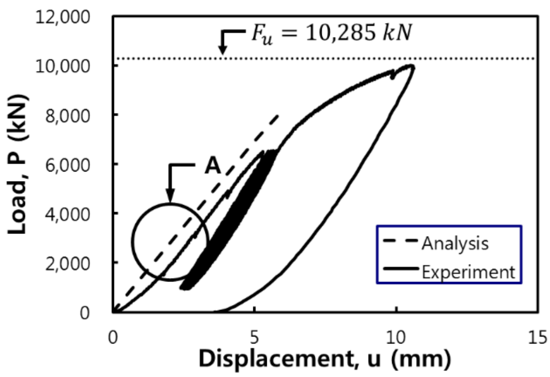

(b) Specimen 2

Fig. 4 Comparison of load-displacement curves

compressive force through the limited area of the anchor head did not produce any meaningful difference in the numerical results.

The FE idealization was validated based on the experimental results. The values of the compressive and tensile strengths of the two specimens were 35 MPa and 3.15 MPa, respectively. The test specimens were designed following the guidelines mentioned in ETAG 013 (EOTA, 2002), which provide details related to the production of the anchorage zone specimen, and a series of KTA-K type anchorage devices developed at RIST (Kwon *et al*. 2015) were used.

All the dimensions in an anchorage device are intimately connected with each other, and the dimensions of the anchorage device height (H_a) and duct hole diameter (b in Fig. 1) depend on the size of the bearing plate (a). The other dimensions related to the spiral reinforcement in Table 1 were determined in advance to be the values that can produce a resisting force F_u according to the anchorage system company (KTA). To prevent failure at the local zone as much as possible, F_u should be close to the ultimate resisting capacity of the anchorage zone developed at the general zone ($F_u = f_c' \times (B \times h - A_{duct})$, where f_c' = compressive strength of the concrete and A_{duct} = area of the duct hole).

Fig. 3 shows representative features of the test setup, and Fig. 4 (a) and (b) represent the obtained load-displacement relations at the bearing plate, where u and P are the axial displacement at point A in Fig. 1 and the corresponding applied load to the bearing plate, respectively.

Since the parametric studies for evaluating the bursting stress and force were conducted using elastic analysis, correlation studies between the experimental data and the numerical analyses were limited to the local level, where severe nonlinear behavior does not develop in the specimens (see Fig. 4).

Regardless of changes in the design variables of the anchorage zone, good agreement was obtained for the individual anchorage blocks, leading to the conclusion that the designed numerical model for the three parts, the concrete matrix, anchorage device, and spiral reinforcement, was sufficiently accurate to predict the elastic behavior of the anchorage zone. A slight difference between the FE analyses and the experimental data at the initial loading stage (ex. Circle A in Fig. 4(b)) appears to have been caused by sliding in the experimental setup due to discordance between the loading axis and the specimen axis (EOTA 2002).

Using the correlation studies between the experimental data of Specimen 1 and the numerical analyses, details for the parametric studies such as the element type, FE mesh size, and loading condition were determined. Finally, the FE model of Specimen 1 was based on our study. The only difference was the length of the specimen, L=1500 mm, which was more than two times the length of Specimen 1.

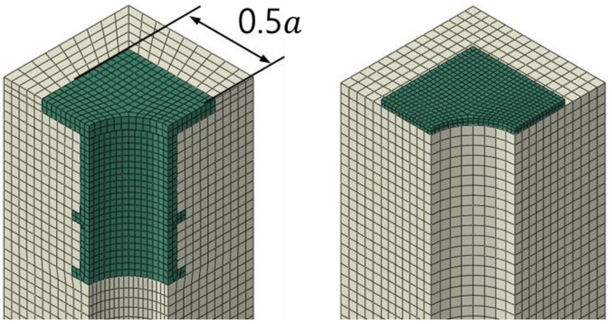

(a) with anchorage device and duct hole (b) with bearing plate and duct hole

Fig. 5 Anchorage block with rectangular bearing plate

Except for the parametric study on the influence of the spiral reinforcement itself, the spiral reinforcement was generally excluded from the numerical modeling in the additional parametric studies because the placement of the spiral reinforcement usually causes a local stress concentration along the spiral, resulting in distortion in the tensile stress distribution along the specimen length. This local stress concentration makes it difficult to accurately quantify the influence of each design parameter on the bursting tensile force.

Two different anchorage blocks used by Kim and Kwak (2018) were considered for the additional parametric study: (1) an anchorage block with an anchorage device and a duct hole (see Fig. 5(a)), and (2) an anchorage block with a duct hole and a bearing plate (see Fig. 5(b)). The reason for including a duct hole is that an anchorage block without a duct hole results in less bursting tensile stress and force than the two anchorage blocks in Fig. 5 (Kim and Kwak 2018). Two different shapes of bearing plate (circular and rectangular) were also considered. When the anchorage bearing plate was changed from a circular shape to a rectangular shape, as shown in Fig. 5, the width of the rectangular bearing plate was assumed to be the same as the diameter of the circular bearing plate. Because previous research was based on 2D analysis, the basic assumption of the previous research was that the shapes of the bearing plate and the concrete block have to be same to express the 3D behavior of the anchorage zone. Because of this, the rectangular bearing plate was modeled to match the shape of the concrete block.

The reliability of the constructed FE model for the anchorage block with the rectangular bearing plate was previously confirmed by comparing the obtained numerical results with those obtained by Burdet (1990). More details can be found in Kim and Kwak (2018).

3. Modification of the AASHTO LRFD equation

The design formula given in the AASHTO LRFD design guidelines (AASHTO LRFD 2012), which was introduced after extensive FE analyses by Burdet (1990), is widely referred to when designing anchorage zones. As shown in Eq. (1), the design formula for evaluating the bursting force mentioned in the AASHTO LRFD design guidelines is

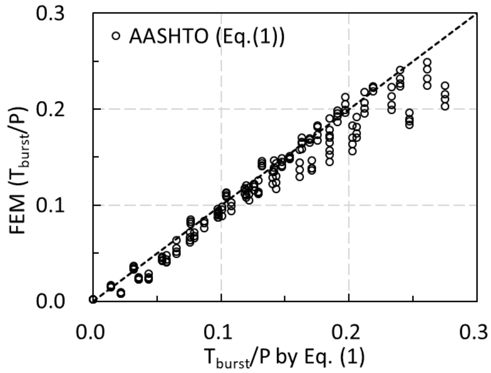

(a) Comparison with AASHTO

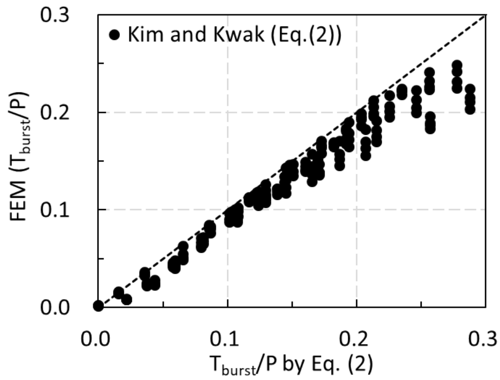

(b) Comparison with Eq. (2)

Fig. 6 Prediction of bursting force using the proposed equation (Kim and Kwak 2018)

composed of two parts. The first part, originally proposed by Mörsch (1924), takes into account the influence of the size of a bearing plate relative to the size of an anchorage block, and the other part concerns the contribution of the inclination of an anchorage device.

$$T_{burst} = 0.25\Sigma P\left(1-\frac{a}{h}\right) + 0.5|\Sigma(P(\sin\alpha)| \qquad (1)$$

where P is the applied prestressing force, a is the bearing plate width, h is the the anchorage block height, and α is the tendon inclination.

Since Eq. (1) was basically developed using 2D FE analysis, it does not have an adequate theoretical basis for considering all the design parameters, and therefore the exactness and reliability of the equation may not be ensured. To examine the reliability of this equation, parametric analyses were performed with the design variables (e.g., the bearing plate size and the duct hole), which increased the bursting force. Then, an improved design equation to evaluate the bursting tensile force in an anchorage block with a rectangular bearing plate was introduced using a modification of Eq. (1).

The introduced modification by Kim and Kwak (2018) concerns the constant of 0.28 in Eq. (2), which corresponds to 0.25 in the formula introduced in the AASHTO LRFD design guidelines. The use of the constant 0.28 stems from the consideration of the duct hole. The comparisons between T_{burst} obtained from the FE analyses and T_{burst} evaluated by Eq. (1) mentioned in AASHTO LRFD and by Eq. (2) introduced by Kim and Kwak (2018) can be found

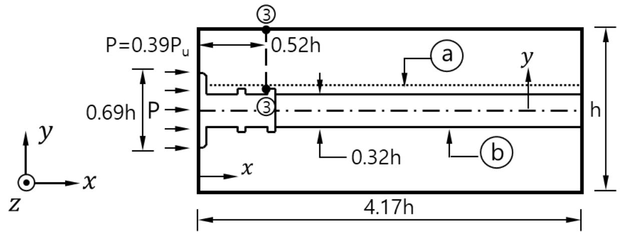

Fig. 7 Section view of the model in Fig. 5(a)

in Fig. 6. As shown in Fig. 6, using Eq. (2) can improve the results obtained by Eq. (1) while reserving the same safety factor. However, the use of Eq. (1) may underestimate the bursting force. Since the basic form and expression of the introduced Eq. (2) are the same as those in Eq. (1), the introduced equation can effectively be used in design practice without any difficulty in application.

$$\mathrm{T}_{burst} = 0.28\Sigma P\left(1 - \frac{a}{h}\right) + 0.5|\Sigma(P(\sin\alpha)| \qquad (2)$$

As mentioned in previous studies (Breen *et al.* 1994, Hou *et al.* 2017), the eccentricity of the bearing plate reduces the bursting force, but the inclination of the tendon increases the bursting force. Because the same results were obtained from the parametric studies, the influence of the eccentricity on the bursting force was excluded when expressing Eq. (2). More details can be found in Kim and Kwak (2018).

4. Influence of trumpets on bursting force

Although Eq. (2) proposed by Kim and Kwak (2018) considered basic influencing factors such as the duct hole, eccentricity and inclination of the tendon, additional parametric studies may need to be conducted to determine whether other influencing factors affect the bursting forces. Accordingly, the influence of a trumpet embedded in a concrete matrix was analyzed first using the FE model in Fig. 5(a).

A typical section of the model is shown in Fig. 7, and the obtained numerical results can be found in Figs. 8-10, where $\sigma_o = P/h^2$ denotes the uniformly distributed basic stress. Sections ⓐ and ⓑ correspond to the point that produces the maximum radial bursting stress σ_y and duct hole surface, respectively. As shown in Fig. 8, the ribs in the trumpet affect the stress distribution while developing additional stress concentration. The maximum bursting stress of $0.26\sigma_o$ is clearly larger than the $\sigma_z^{max} = 0.14\sigma_o$, which was developed when the duct hole was ignored, but not much larger than the $\sigma_z^{max} = 0.23\sigma_o$ obtained when the duct hole was considered (Kim and Kwak 2018). In any case, the variation in the maximum spalling stress on the surface is not very large. This means that the stress concentration developed at the trumpet rib only shows a local effect, which induces from the rib placement.

The distribution of bursting stress along the anchorage zone does not govern bursting force (see Fig. 9(a)), which is determined by integrating the bursting stress distribution. The evaluated bursting force of $T_{burst} = 0.046P$ is rather small compared with the $T_{burst} = 0.085P$ obtained when the trumpet was excluded, as shown in Fig. 5(b). This result means that the influence of the trumpet can be ignored and the simpler FE model in Fig. 5(b) can be used for the evaluation of the bursting forces. That is, the influence of the trumpet does not need to be included in the expression of the design equations (see Eqs. (1) and (2)).

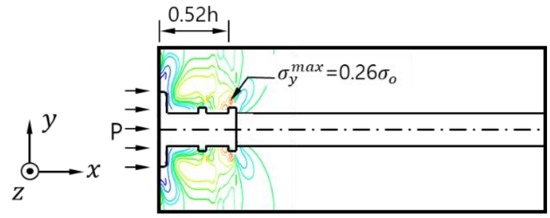

(a) Radial direction (y-axis)

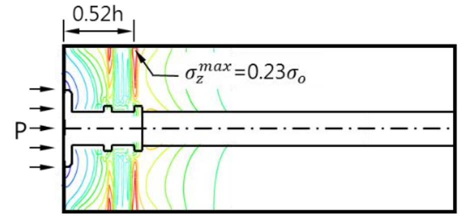

(b) Tangential direction (z-axis)

Fig. 8 Bursting stress contours of the model in Fig. 5(a)

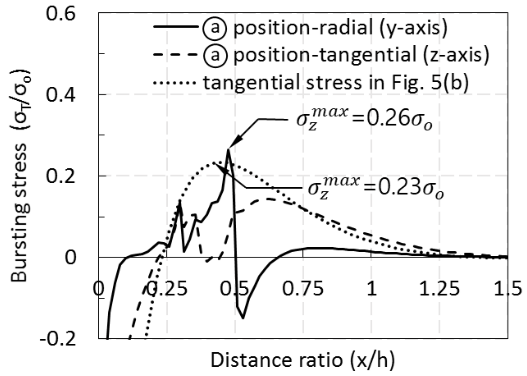

(a) Stress distribution along ⓐ position

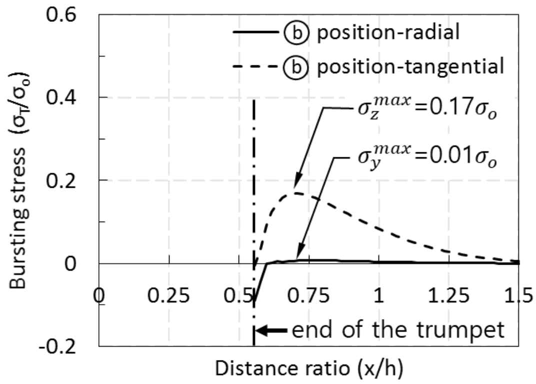

(b) Stress distribution along ⓑ position

Fig. 9 Bursting stress distribution along ⓐ and ⓑ positions in Fig. 7

5. Influence of multiple anchorage devices

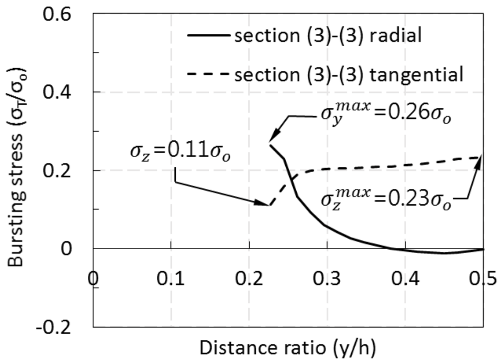

Fig. 10 Bursting stress distribution across the depth (See Fig. 8)

To investigate the effect of multiple anchorage devices, Yettram and Robin (1970) performed 3D FE analyses for an anchorage block without a duct hole, and the obtained results were compared with those for a single anchorage device. The final conclusion was that the bursting stress developed with multiple anchorage devices was smaller than that of a single anchorage device. Breen *et al*. (1994) also analyzed anchorage blocks with multiple anchorage devices using the strut-and-tie model, and concluded that since the forces are already distributed over the cross section, the bursting stress becomes less critical with an increasing number of anchorage devices.

Nevertheless, we performed an additional parametric study to check whether the multiple anchorage device effect was still effective in the 3D FE analyses considering a duct hole. Usually, with multiple anchorages, the individual anchorages are placed side-by-side with enough spacing between the anchorage devices (Yettran and Robin 1970). To examine the change in the bursting stress components according to the number of anchorage devices, two typical multiple anchorage configurations were considered. The bursting stresses along points ⓒ, ⓓ, and ⓔ in Fig. 11 were compared because each stress was expected to be different due to the interference of the adjacent anchorage zone.

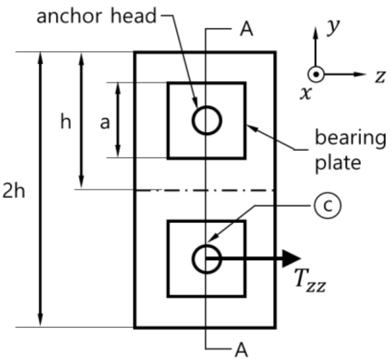

(a) Two anchorages

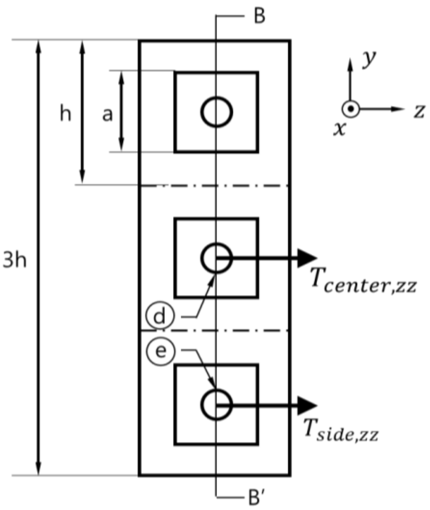

(b) Three anchorages

Fig. 11 End face of multiple anchorage configurations

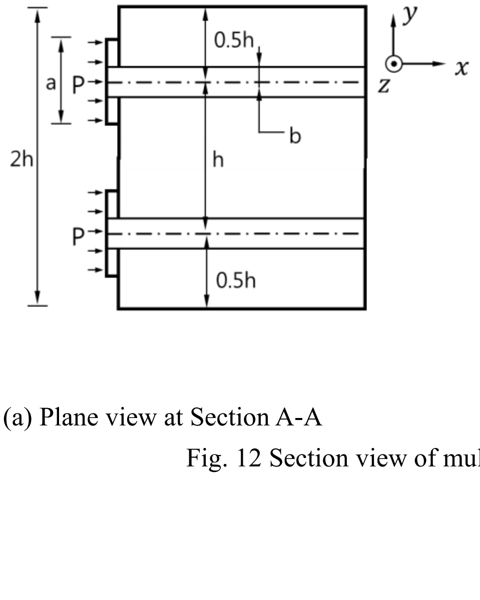

(a) Plane view at Section A-A

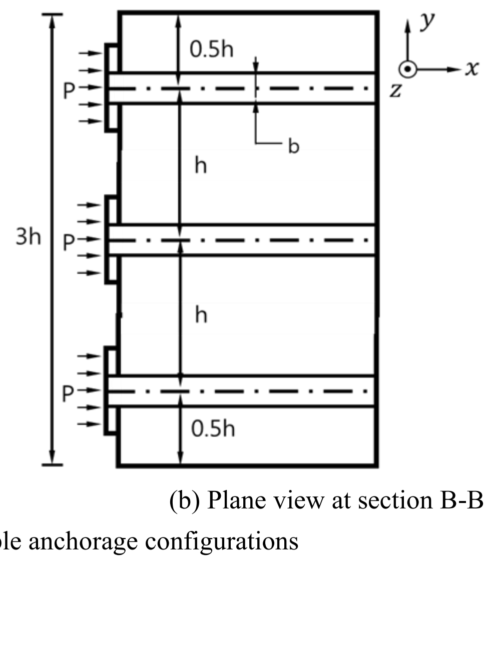

(b) Plane view at section B-B

Fig. 12 Section view of multiple anchorage configurations

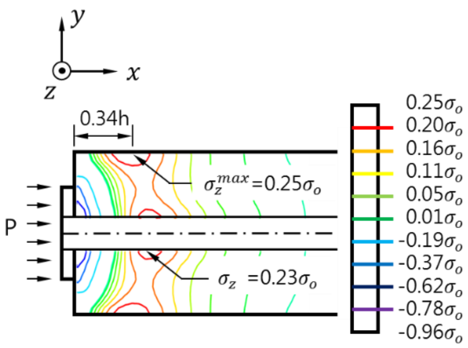

(a) Tangential stress (*x*-*y* section)

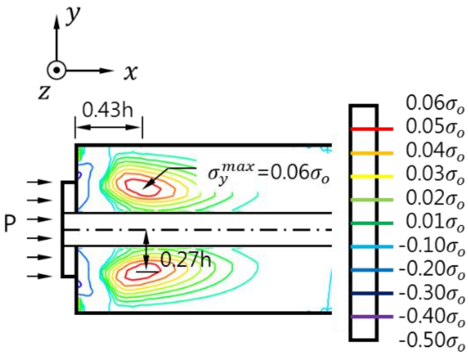

(b) Radial stress (*x*-*y* section)

Fig. 13 Bursting stress at a single anchorage placement (Kim and Kwak 2018)

The reference planes used to determine the bursting stresses and forces are described in Figs. 11 and 12. The duct hole diameter was assumed to be b=114 mm, and the typical locations ⓒ to ⓔ described by letters within parentheses correspond to the duct hole surface. 3D FE analyses were conducted, adopting the same mesh size as that used for a single anchorage device.

For comparison with the numerical results, the results obtained for a single anchorage placement with a=250 mm and h=360 mm are described again in Fig. 13 as a reference value. More details for the change in the structural behavior of an anchorage block according to consideration of a duct hole can be found in Kim and Kwak (2018). Figs. 14 and 15 represent the stress contour lines and the stress distribution along the length direction in the anchorage block with two anchorage devices, in which the dimensions for bearing plate width (a) and concrete block width (h) in Fig. 14 are the same as those considered in Fig. 13. As shown in Fig. 14(a), the maximum tangential bursting stress directed to the z-axis ($\sigma_z^{max} = 0.28\sigma_o$) is larger than the stress $\sigma_z^{max} = 0.23\sigma_o$ obtained at the anchorage block for a single anchorage device (see Fig. 13). However, the tangential bursting stresses through the entire section seem to be smaller than those for the single anchorage device due to the restriction of the transverse spreading of applied axial force P as mentioned by many previous researchers (Yettram and Robbins 1970, Burdet 1990, Breen *et al.* 1994).

In addition, the bursting stresses σ_y in the radial direction (see Fig. 14(b)) are still smaller than the tangential bursting stress σ_z, as was the case with a single anchorage

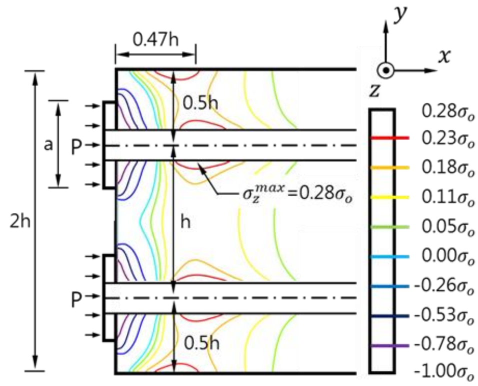

(a) Tangential stress (*x*-*y* section)

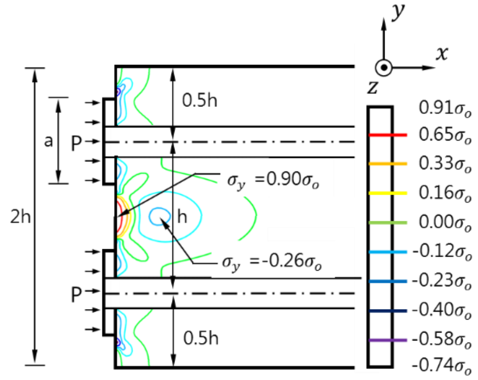

(b) Radial stress (*x*-*y* section)

Fig. 14 Bursting stress contours developed at two anchorage devices when a=250 mm and h=360 mm

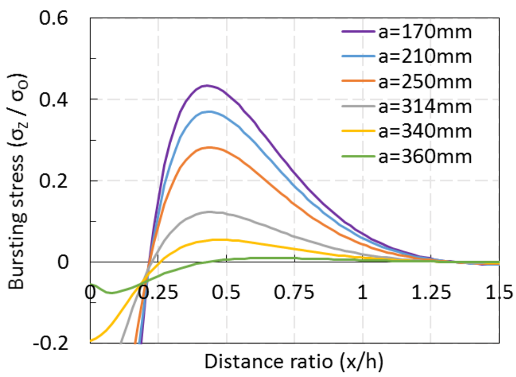

(a) Tangential stress distribution at point ⓒ in Fig. 11

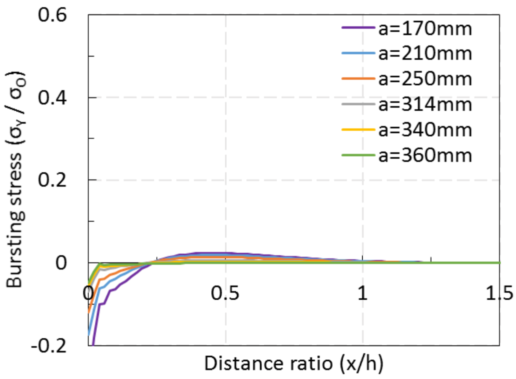

(b) Radial stress distribution at point ⓒ in Fig. 11

Fig. 15 Bursting stress distribution along tendons with two anchorages (Fig. 11 (a))

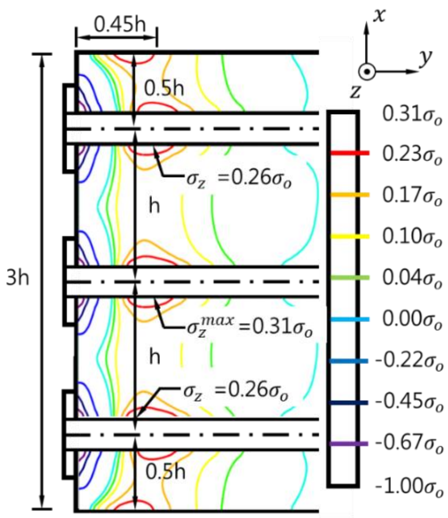

(a) Tangential stress (*x*-*y* section)

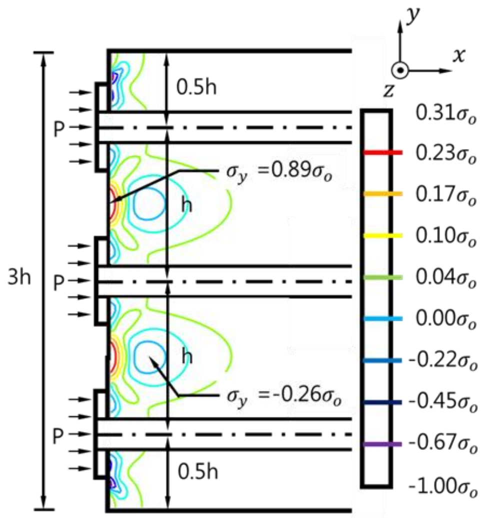

(b) Radial direction (*x*-*y* section)

Fig. 16 Bursting stress contours developed for three anchorage devices

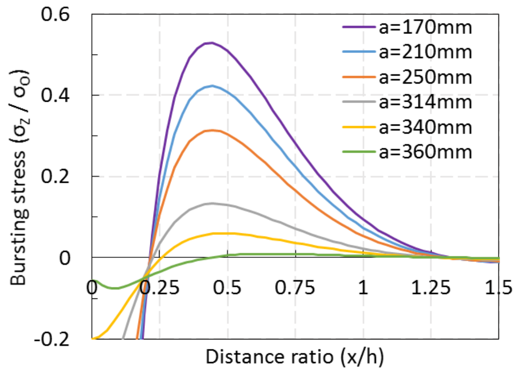

(a) Tangential stress distribution at point ⓓ in Fig. 11

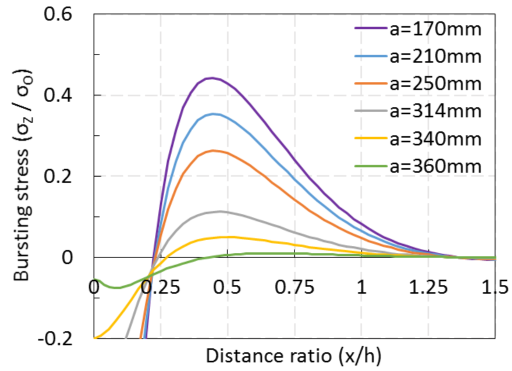

(b) Tangential stress distribution at point ⓓ in Fig. 11

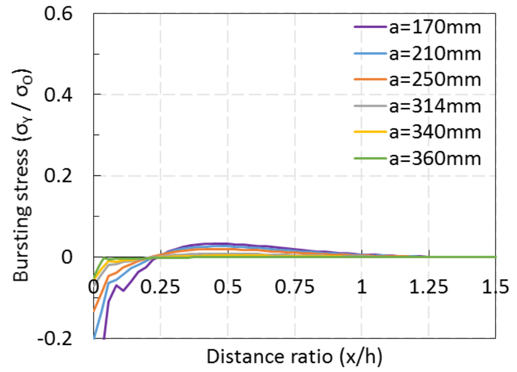

(c) Radial stress distribution at point ⓓ in Fig. 11

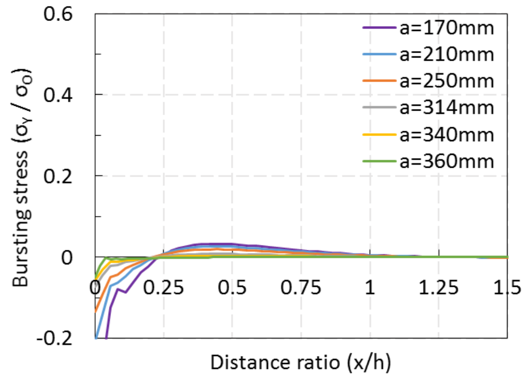

(d) Radial stress distribution at point ⓔ in Fig. 11

Fig. 17 Bursting stress distribution along tendons with three anchorages

device. Unlike the case of a single anchorage device, however, the radial bursting stress σ_y in the y-direction represents a compressive stress of $\sigma_y = -0.26\sigma_o$ in the central region between both anchorage devices because the expansion of the concrete matrix has been prevented (see Fig. 14(b)).

Additional parametric studies after changing the size of the bearing plate also show the same results as those of a single anchorage device, which represents a reduction in bursting stress with an increase in anchorage plate size (see Fig. 15). This tendency remains even in the case of three anchorage devices; the obtained results are displayed in Figs. 16 and 17.

To determine why the bursting stress that developed at multiple anchorage placements is larger than that for a single anchorage placement, two different loading cases were applied to the two anchorage devices model, with a bearing plate of *a*=250 mm. The load was applied to one

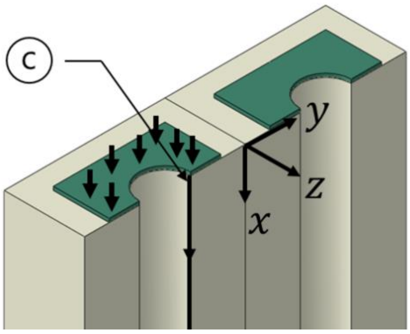

(a) loading case 1

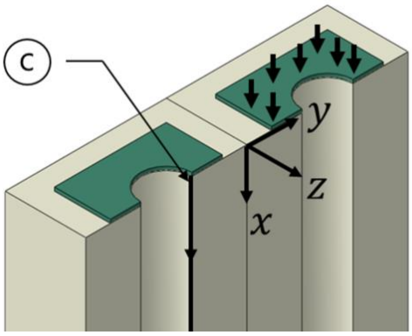

(b) loading case 2

Fig. 18 Loading cases for the two anchorage zone systems

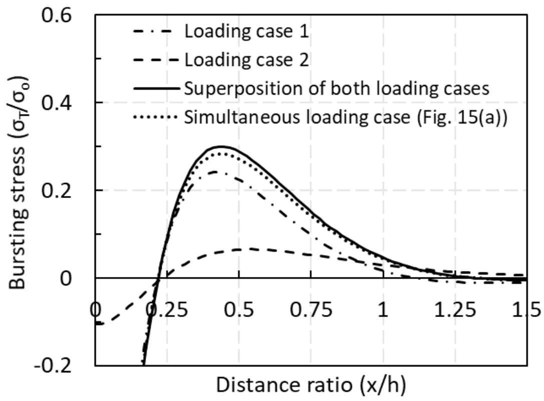

Fig. 19 Bursting stress distribution along the position ⓒ when a=250 mm

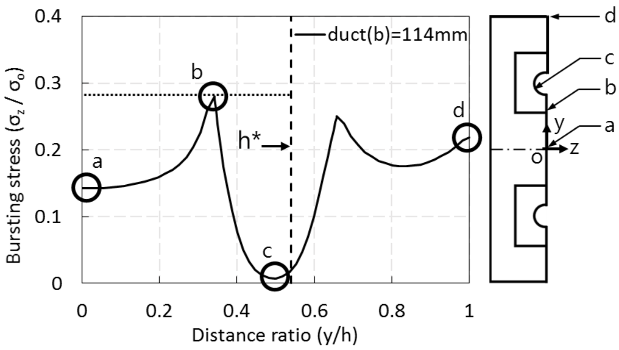

(a) σ_z stress distribution for two anchorage devices

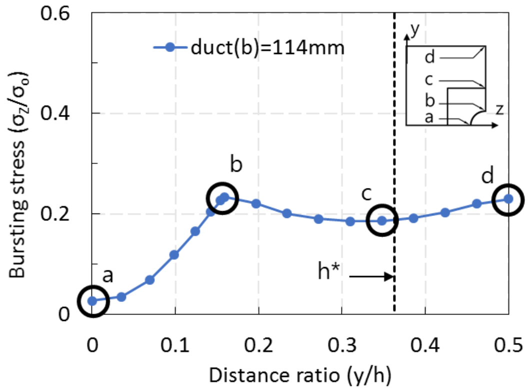

(b) σ_z stress distribution for one anchorage zone system

Fig. 20 Tangential bursting stress distribution across depth

bearing plate first and then to the next bearing plate, as shown in Fig. 18. Loading case 2 describes the situation where the prestressing force was only applied to the adjacent anchorage zone. The tangential bursting stress along location ⓒ was evaluated for each loading case, and Fig. 19 shows its distribution along the length.

As shown in this figure, loading case 1 produces lower stress values than the simultaneous loading of a single anchorage device with a=250 mm in Fig. 15(a) due to the eccentricity effect. Loading case 2 also develops a bursting stress, even though position ⓒ is far from the loaded anchorage zone. When the results of the two loading cases are superposed, the bursting stress distribution is slightly larger than that of the simultaneous loading case (see Fig. 15(a)). This difference seems to be caused by the eccentricity effect that occurred in loading cases 1 and 2, because these two loading cases have eccentric loads in the anchorage zone. This leads to increases in the bursting stress distribution.

On the other hand, while the bursting force can be evaluated by integrating the bursting stresses, the existence of the duct hole produces a non-uniform distribution in the tangential bursting stresses σ_z across the depth in the model at x=0.47h, where the maximum bursting stress σ_z^{max} is developed. Fig. 20 shows bursting stress distribution in the y-direction. Accordingly, to evaluate the bursting force, the duct hole has to be considered (Kim and Kwak 2018). As already mentioned, previous studies have reported that bursting stress developed with multiple anchorage devices is less than that of a single anchorage device, and hence, the bursting force of the single anchorage device will be the most critical for the anchorage block.

Unlike previous design equations that were based on 2D analyses and assumed a constant distribution of bursting stress across the depth (the y-direction in Fig. 20), the numerical results of the 3D FE analyses show that the bursting stress across the depth is not constant but varies rapidly due to the existence of the duct holes. This means that determining the bursting force needs to be accomplished after evaluating the equivalent depth, which corresponds to the assumption of constant bursting stress distribution.

Since the normalized bursting stresses along the length at each location in Fig. 20 are almost the same (see Fig. 21), the equivalent depth h^* can be evaluated by the relation $h^* = \int \sigma_z dy / \sigma_z^{max}$, which takes into account the stress

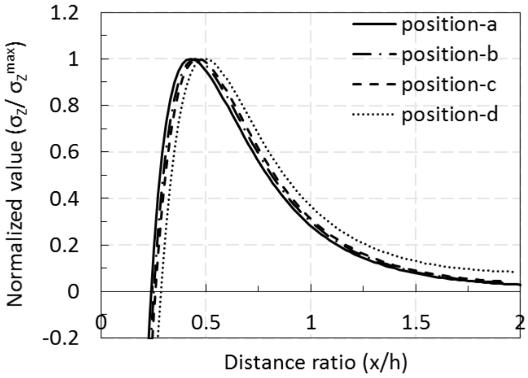

Fig. 21 Tangential bursting stress distribution along the length in Fig. 20(a)

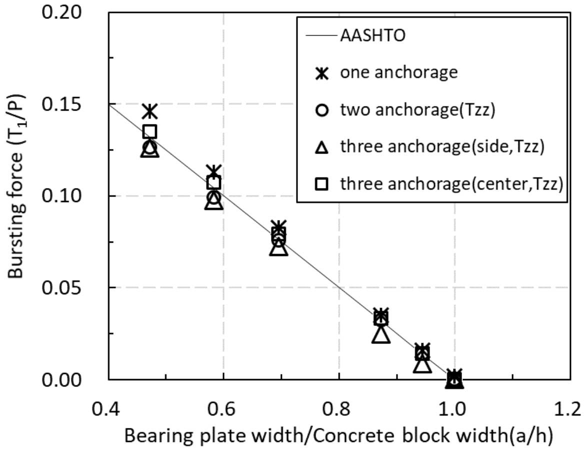

Fig. 22 Bursting force in the anchorage block with multiple anchorage devices

variation across the depth, where σ_z^{max} means the maximum bursting stress at its own position. Then, the bursting force can be determined by integrating the bursting stress along the length $T_{burst} = \int \sigma_z dx h^*$.

Based on the parametric studies with varying sizes of duct hole, the evaluated bursting forces for multiple anchorage devices are shown in Fig. 22. Even though the bursting stress for multiple anchorage devices is slightly larger than that of the single anchorage device, the bursting force for multiple anchorage devices is lowered by a considerable reduction in bursting stress across the depth. The bursting forces for one anchorage device are therefore slightly larger than those for multiple anchorage devices, and this means that the influence of the multiple anchorage devices can be excluded from the evaluation of bursting forces in the design.

6. Influence of spiral reinforcement

Most anchorage devices incorporate spiral reinforcement behind the bearing plate to confine the concrete and hence improve its bearing capacity. This means that development of the bursting tensile force will be suppressed in the core area of the concrete within the spiral reinforcement. To evaluate the influence of spiral reinforcement, an additional parametric study was performed for the same specimen used in Fig. 5(b). The only difference with Specimen 1 in Table 1, which was based on previous parametric studies, was the placement of the spiral reinforcement.

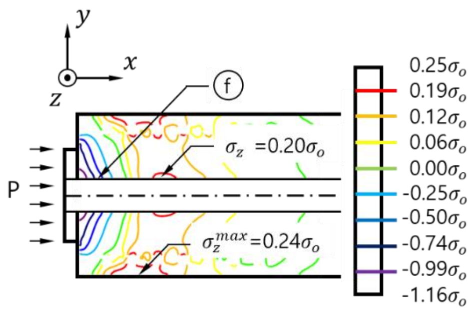

(a) Tangential stress (x-y section)

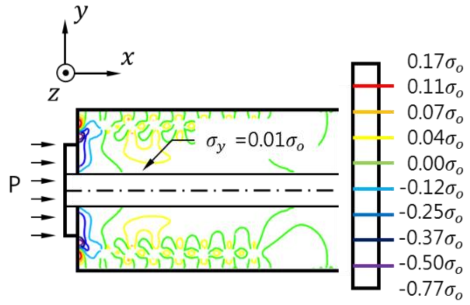

(b) Radial stress (x-y section)

Fig. 23 Bursting stress contour for anchorage with spiral reinforcement

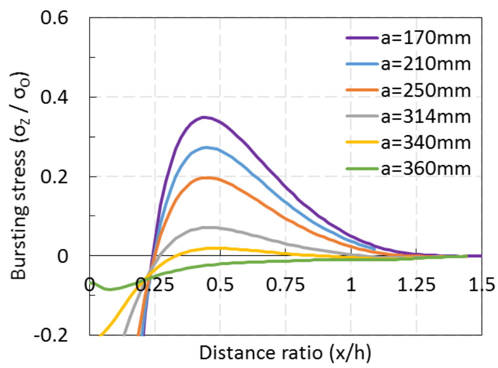

(b) Tangential stress distribution along ⓕ (see Fig. 23(a))

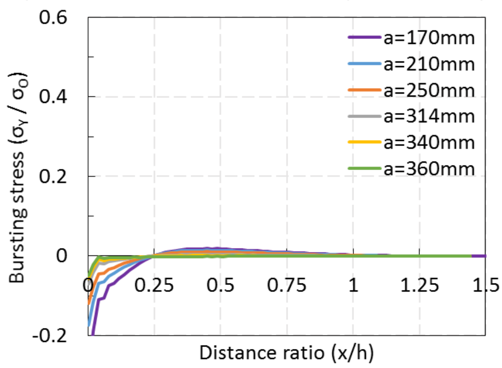

(b) Radial stress distribution along ⓕ (see Fig. 23(a))

Fig. 24 Bursting stress distribution for anchorage with spiral reinforcement

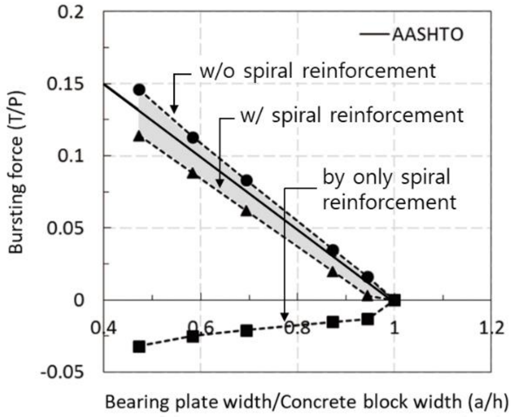

Fig. 25 Bursting force in the anchorage block with spiral reinforcement

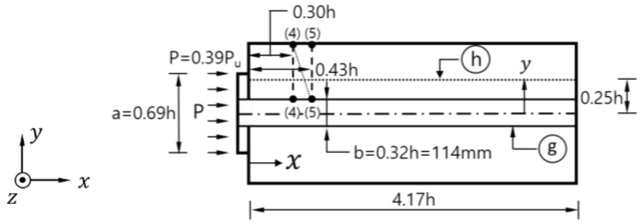

Fig. 26 Section view of the model in Fig. 5(b)

Figs. 23 and 24 show the stress contour lines and the stress distributions along the length direction. As was expected for the spiral reinforcement, Fig. 23 shows a decrease in bursting stresses in both the tangential and radial directions when the stresses are compared with those in Fig. 13. Stress distortion also occurs at the spiral reinforcement position, but Fig. 24 shows that the bursting stress distribution along the duct hole surface is not distorted. Fig. 25 shows the bursting forces as determined by the parametric studies. With the various sizes of bearing plate, the spiral reinforcement reduces the bursting force, and the reduction amount is an almost constant value of $0.025 \cdot T_{bursting}/P$ regardless of the size of the bearing plate. This result seems to depend on the placement of the spiral reinforcement regardless of the plate size. From the obtained results, it can be concluded that the influence of the spiral reinforcement does not need to be considered in the evaluation of bursting force in the design.

7. Influence of circular bearing plate

While proposing an improved equation to determine the bursting force in the previous study (Kim and Kwak 2018), rectangular bearing plates considered in the anchorage device were based. This is because many design equations including those used in the AASHTO LRFD design guidelines were proposed through the analysis results obtained from 2D analyses in which the shape of the bearing plate cannot be considered. Recently, however, since circular bearing plate anchorage devices are also frequently used with various post-tensioning members, the influence of the circular bearing plate needs to be examined.

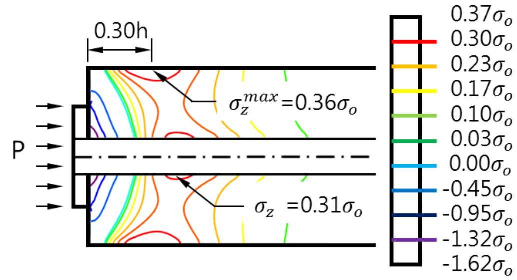

(a) Tangential stress (x-y section)

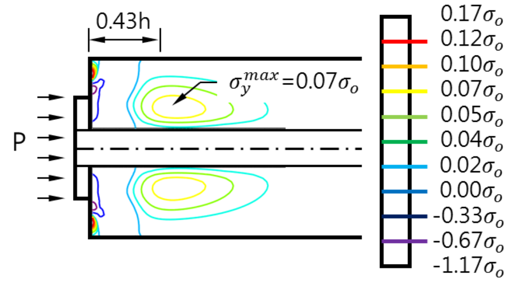

(b) Radial stress (x-y section)

Fig. 27 Bursting stress contour for anchorage with a circular bearing plate

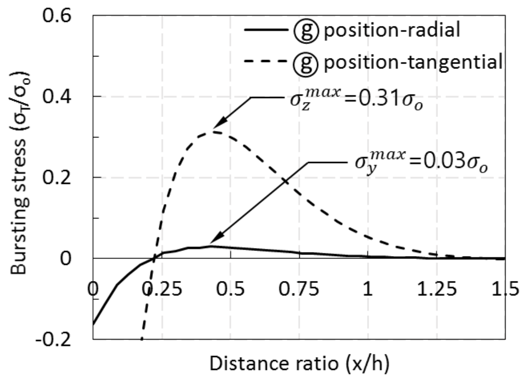

(a) Stress distribution at position ⓖ

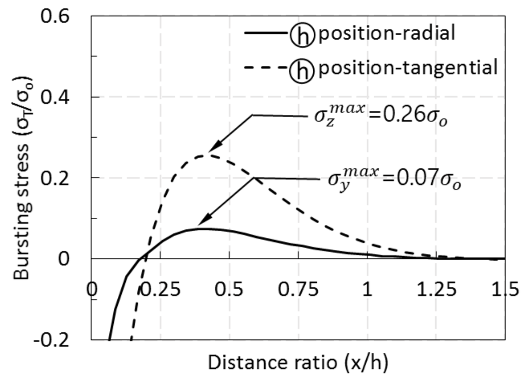

(b) Stress distribution at position ⓗ

Fig. 28 Bursting stress distribution for anchorage with a circular bearing plate

First, parametric studies were performed for a rectangular anchorage block with a circular bearing plate, using the same solution procedures as those for a rectangular bearing plate (Kim and Kwak 2018). Hence, except for the change in the shape of the bearing plate, the

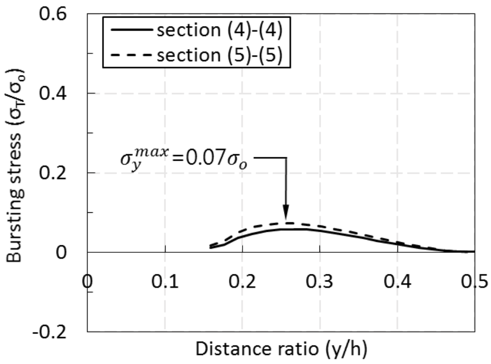

(a) Radial bursting stress distribution

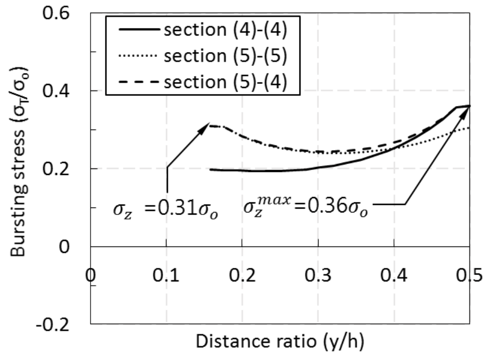

(b) Tangential bursting stress distribution

Fig. 29 Bursting stress distribution for anchorage with a circular bearing plate

same specimens used for the 3D FE analyses were considered for comparison with the numerical results for the rectangular bearing plate. A typical section of the model is shown in Fig. 26. More details of the specimen can be found in Kim and Kwak (2018).

Figs. 27 and 28 represent the stress contour lines and the stress distributions along the length direction for the corresponding bursting stresses, when the diameter of the duct hole was b=114 mm, and a/h=0.69 (see Fig. 26). As with the anchorage block with the rectangular bearing plate, the tangential bursting stress σ_z is based on the bursting force because the magnitude of the radial bursting stress σ_y is very small, as shown in Fig. 28. However, the use of the circular bearing plate causes an increase in stresses compared with the rectangular bearing plate. The maximum tangential bursting stress increases to $\sigma_z = 0.31\sigma_o$, which is about 30% larger than the maximum bursting stress of the $\sigma_z = 0.23\sigma_o$ obtained for the anchorage block with the rectangular bearing plate, shown in Fig. 13(a). In addition, as shown in Fig. 29, the tangential bursting stresses across the depth still maintain a uniform distribution, as was the case with the rectangular bearing plate in Kim and Kwak (2018).

After determining the bursting stresses, the same solution procedures used for the anchorage block with the rectangular bearing plate were used to obtain the bursting force. Fig. 30 shows the evaluated bursting forces according to the change in the diameter of the bearing plate. As shown in the figure, the design guideline in Eq. (1) proposed for the anchorage block with the rectangular bearing plate

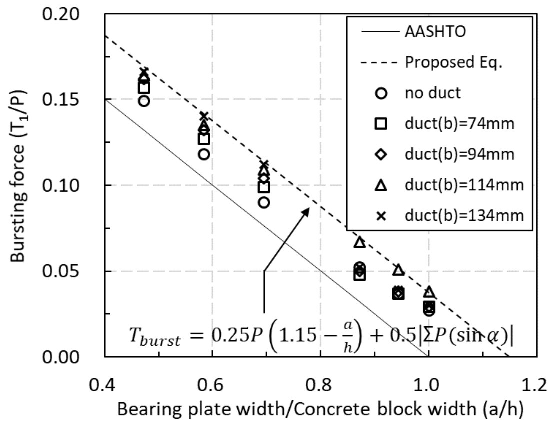

Fig. 30 Bursting force in the anchorage block with a duct hole

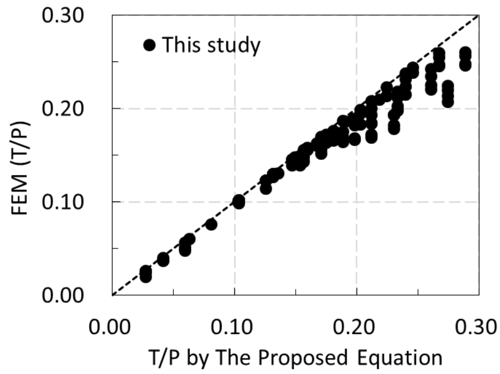

(a) Comparison between finite element method (FEM) and proposed equation

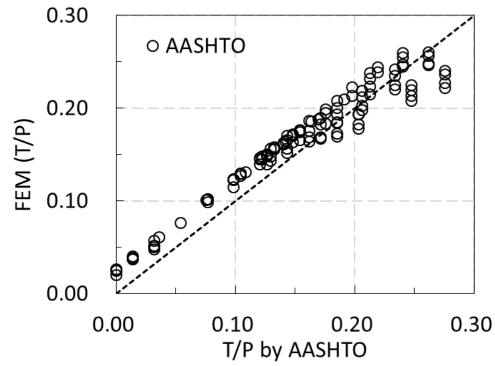

(b) Comparison between finite element method (FEM) and AASHTO

Fig. 31 Prediction of bursting force using the proposed Eq. (3)

seems to be insufficient for the circular bearing plate. Specifically, when the ratio of the diameter of the bearing plate to the anchorage block height (a/h) is 1.0, a portion of the bursting force is developed, and this magnitude is maintained through the entire range of the bearing plate size. This difference is attributed to the fact that the circular bearing plate cannot cover the entire concrete anchorage block, even in the case of a/h=1.0, and this situation leads to the development of bursting stresses.

The design equation in Eq. (1), which was introduced for the anchorage block with the rectangular bearing plate consequently needs to be modified to be applied to a rectangular anchorage block with a circular bearing plate. This additional modification was performed for Eq. (1), and Eq. (3) is newly introduced, based on the linear regression of the numerical results for the circular bearing plate.

$$\mathrm{T}_{burst} = 0.25\Sigma P\left(1.15 - \frac{a}{h}\right) + 0.5|\Sigma(P(\sin\alpha)| \qquad (3)$$

Fig. 31 shows the results of correlation studies between the design equations and the 3D analysis results. They show that the AASHTO LRFD design guidelines may underestimate bursting forces. This underestimation results from not considering the influence of a duct hole and the shape of the bearing plate. Eq. (3) provides improved results when determining the bursting force for an anchorage block with a circular bearing plate. Finally, to address the inaccuracy of the AASHTO LRFD design guidelines, which do not consider the influence of a duct hole or the shape of the bearing plate, Eq. (2) for the rectangular bearing plate and Eq. (3) for the circular bearing plate can be effectively used for determining the reinforcement for the bursting force.

8. Conclusions

Using 3D FE analysis, design equations were proposed to evaluate the bursting forces in the anchorage zone of post-tensioned members, and their validity was determined by comparison with the AASHTO LRFD design equation, which is widely applied in structural design. The influences of components comprising the anchorage zone were also examined. These design components included the trumpet in the anchorage device, multiple anchorage zone systems, the spiral reinforcement, and the circular bearing plate on the rectangular anchorage block. The additional numerical analyses yielded the following conclusions: (1) A trumpet embedded in a concrete matrix increases the maximum bursting stress, but it has a local effect, which does not affect the evaluation of a bursting force. (2) A bursting force developed in a multiple anchorage system decreases because the transverse spreading of the bursting stresses is restricted. (3) Spiral reinforcement reduces the bursting force because of the confinement effect. (4) A circular bearing plate produces a larger bursting force than a rectangular bearing plate. These findings around the influences of the components on the bursting force are in good agreement with results obtained in previous studies (Yettran and Robin 1970, Breen *et al*. 1994, Rogowsky and Marti 1996, Zhou *et al*. 2015). Furthermore, since a trumpet decreases the bursting force, the proposed equation will predict the bursting force safely regardless of anchorage device type. The introduced design equations (Eqs. (2) and (3)) can be used for determining the amount of reinforcing steel to resist bursting stresses in an anchorage block.

Acknowledgment

This work is supported by a Korea Agency for Infrastructure Technology Advancement (KAIA) grant funded by the Ministry of Land, Infrastructure and Transport (Grant 13IFIP-C113546-01), and Korea Ministry of Land, Infrastructure and Transport(MOLIT) as 「Innovative Talent Education Program for Smart City」.

References

AASHTO (2012), AASHTO LRFD Bridge Design Specifications, America Association of State Highway Transportation Officials, Washington, DC, USA

Adeghe, L.N. and Collins, M.P. (1987), “A finite element model for studying reinforced concrete detailing problems”, Ph.D. Dissertation, The University of Toronto, Toronto, Canada.

Al-saadoun, S.S. (1980), “A Three-dimensional photoelastic investigation of the stress distribution in the anchorage zone of post-tensioned beams”, Master Dissertation, King Fahd University of Petroleum and Minerals, Dhahran, Saudi Arabia.

American Concrete Institute Committee 318 (2014), ACI 318-14 Building Code Requirements for Structural Concrete and Commentary, Structural Building Code, Farmington Hills, MI, USA.

Breen, J.E., Burdet, O., Roberts, C., Sanders, D. and Wollmann, G. (1994), *Anchorage Zone Reinforcement for Post-tensioned Concrete Girders*, Transportation Research Board, Washington (DC), USA.

Burdet, O. (1990), “Analysis and design of anchorage zones in post-tensioned concrete bridges”, Ph.D. Dissertation, The University of Texas, Austin, USA.

CEB-FIP Model Code (2010), Fib Model Code for Concrete Structures, Committee Euro-International du Beton, Lausanne, Switzerland

Choi, K. and Lho, B. (2015), “Study on bursting stress in anchorage zone of prestressed concrete using circular anchorages”, *J. Korea Inst. Struct. Mainten. Inspect.*, **19**(1), 3-12. https://doi.org/10.11112/jksmi.2015.19.1.003.

Choi, K.C., Park, Y.H. and Paik, I.Y. (2010), “Evaluation of bursting behavior in anchorage zone of PSC I girders”, *J. Korean Soc. Civil Eng.*, **30**(3), 329-336.

Dassault Systèmes (2013), “ABAQUS online user manual version 6.13-1”, Dassault Systèmes, Waltham, MA.

den Uijl, J.A. (1983), “Tensile stresses in the transmission zones of hollow-core slabs prestressed with pretensioned strands”, Delft University of Technology, Stevin Laboratory, Delft, Netherlands.

Douglas, D.J. and Trahair, N.S. (1960), “An examination of the stresses in the anchorage zone of a post-tensioned prestressed concrete beam”, *Mag. Concrete Res.*, **12**(34), 9-18. https://doi.org/10.1680/macr.1960.12.34.9.

EOTA (European Organisation for Technical Approvals) (2002), “ETAG 013: Guideline for European technical approval of post-tensioning kits for prestressing of structures”, EOTA, Brussels, Belgium

Fenwick, R.C. and Lee, S.C. (1986), “Anchorage zones in prestressed concrete members”, *Mag. Concrete Res.*, **38**(135), 77-89. https://doi.org/10.1680/macr.1986.38.135.77.

Haroon, S., Yazdani, N. and Tawfiq, K. (2006), “Posttensioned anchorage zone enhancement with fiber-reinforced concrete”, *J. Bridge Eng.*, **11**(5), 566-572. https://doi.org/10.1061/(ASCE)1084-0702(2006)11:5(566).

He, Z. and Liu, Z. (2011), “Investigation of bursting forces in anchorage zones: compression-dispersion models and unified design equation”, *J. Bridge Eng.*, **16**(6), 820-827. https://doi.org/10.1061/(ASCE)BE.1943-5592.0000187.

Hou, D.W., Zhao, J.L., Shen, J.S.L. and Chen, J. (2017), “Investigation and improvement of strut-and-tie model for design of end anchorage zone in post-tensioned concrete structure", *Constr. Build. Mater.*, **136**, 482-494. https://doi.org/10.1016/j.conbuildmat.2017.01.033.

Jo, B., Byun, Y. and Tae, G. (2002), "Structural behavior of cable anchorage zones in prestressed concrete cable-stayed bridge", *Can. J. Civil Eng.*, **29**(1), 171-180. https://doi.org/10.1139/l01-087.

Kara, M.E., Firat, F.K., Sonmez, M. and Karabork, T. (2016), "An investigation of anchorage to the edge of steel plates bonded to RC structures", *Steel Compos. Struct.*, **22**(1), 25-43. https://doi.org/10.12989/scs.2016.22.1.025.

Kim, J., Yang, J. and Kwon, Y. (2016), "Influence of steel fiber and reinforcing details on the ultimate bearing strength of the post-tensioning anchorage zone", *Struct. Eng. Mech.*, **59**(5), 867-883. https://doi.org/10.12989/sem.2016.59.5.867.

Kim, J.K., Kwon, Y. and Kwak, H.G. (2014), "Anchorage zone behavior in the slab with flat anchorage", *J. Korean Soc. Hazard Mitig.*, **14**(1), 67-76. https://doi.org/10.9798/KOSHAM.2014.14.1.67.

Kim, J.K., Yang, J.M. and Yim, H.J. (2016), "Experimental evaluation of transfer length in pretensioned concrete beams using 2,400-MPa prestressed strands", *J. Struct. Eng.*, **142**(11), 4016088. https://doi.org/10.1061/(ASCE)ST.1943-541X.0001567.

Kim, J.R and Kwak, H.G. (2018), "FE analyses and prediction of bursting forces in post-tensioned anchorage zone", *Comput. Concrete*, **21**(1), 75-85. https://doi.org/10.12989/cac.2018.21.1.075.

Kwon, Y.S., Kim, J.K. and Kwak, H.G. (2015), "Ultimate strength of anchorage zone according to geometric parameters of post-tensioning anchorage using a finite element method", *J. Comput. Struct. Eng. Inst. Korea*, **28**(3), 317-324. https://doi.org/10.7734/COSEIK.2015.28.3.317.

Liu, C., Xu, D., Jung, B. and Morgenthal, G. (2013), "Reinforcement design for the anchorage of externally prestressed bridges with 'tensile stress region'", *Comput. Concrete*, **11**(5), 383-397. https://doi.org/10.12989/cac.2013.11.5.383.

Marchão, C., Lúcio, V. and Ganz, H.R. (2019), "Efficiency of the confinement reinforcement in anchorage zones of posttensioning tendons", *Struct. Concrete*, **20**(3), 1182-1198. https://doi.org/10.1002/suco.201800238.

O'Callaghan, M.R. and Bayrak, O. (2008), "Tensile stresses in the end regions of pretensioned I-beams at release", Master Dissertation, The University of Texas, Austin, USA.

Oh, B.H. and Lim, D.H. (1995), "Stress distribution and crack control at anchorage zones in prestressed concrete box-girder bridge members", *J. Korean Soc. Civil Eng.*, **15**(2), 325-336.

Oh, B.H., Lim, D.H. and Park, S.S. (1997), "Stress distribution and cracking behavior at anchorage zones in prestressed concrete members", *ACI Struct. J.*, **94**(5), 549-557.

Okumus, P., Oliva, M.G. and Becker, S. (2012), "Nonlinear finite element modeling of cracking at ends of pretensioned bridge girders", *Eng. Struct.*, **40**, 267-275. https://doi.org/10.1016/j.engstruct.2012.02.033.

Robinson, B., Florida, A., Tawfiq, K.S. and Engineering, F.C. (2009), "Using steel fiber reinforced concrete in post-tensioned anchorage zones", *Structures Congress 2009*, Austin, Texas, USA, May.

Sahoo, D.K., Singh, B. and Bhargava, P. (2009), "Investigation of dispersion of compression in bottle-shaped struts", *ACI Struct. J.*, **106**(2), 178-186.

Sanders, D.H. and Breen, J.E. (1997), "Post-tensioned anchorage zones with single straight concentric Anchorages", *ACI Struct. J.*, **94**(2), 146-158.

Schlaich, J., Schäfer, K. and Jennewein, M. (1987), "Toward a consistent design of structural concrete", *PCI J.*, **32**(3), 74-150.

Shen, S.L., Hou, D.W., Zhao, J.L., Horpibulsuk, S. and Yin, Z.Y. (2014), "Assessment of internal forces for intermediate anchorage zone of post-tensioned concrete structure", *Constr. Build. Mater.*, **64**, 370-378. https://doi.org/10.1016/j.conbuildmat.2014.04.085.

Songwut, H. (2004), "Linear and nonlinear finite element analyses of anchorage zones in post-tensioned concrete structures", Ph.D. Dissertation, Virginia Polytechnic Institute and State University, Blacksburg, USA.

Stone, W.C. and Breen, J.E. (1984), "Behavior of post-tensioned girder anchorage zones", *PCI J.*, **29**(1), 64-109.

Sundara Raja Iyengar, K.T. and Yogananda, C.V. (1966), "A three-dimensional stress distribution problem in the anchorage zone of a post-tensioned concrete beam", *Mag. Concrete Res.*, **18**(55), 75-84. https://doi.org/10.1680/macr.1966.18.55.75.

Wollmann, G.P. (1992), "Anchorage zones in post-tensioned concrete structure", Ph.D. Dissertation, The University of Texas, Austin, USA.

Wollmann, G.P., Breen, J.E. and Kreger, M.E. (2000), "Anchorage of external tendons in end diaphragms", *J. Bridge Eng.*, **5**(3), 208-215. https://doi.org/10.1061/(ASCE)1084-0702(2000)5:3(208).

Yettram, A.L. and Robbins, K. (1970), "Anchorage zone stresses in post-tensioned uniform members with eccentric and multiple anchorages", *Mag. Concrete Res.*, **22**(73), 209-218. https://doi.org/10.1680/macr.1970.22.73.209.

Yun, Y.M. (2005), "Evaluation of ultimate strength of post-tensioned anchorage zones", *J. Adv. Concrete Technol.*, **3**(1), 149-159. https://doi.org/10.3151/jact.3.149.

Zhao, J.L., Shen, S.L., Wang, L.B. and Chen, J. (2011), "A design approach for the interior anchorage zone of post-tensioned concrete structure", *KSCE J. Civil Eng.*, **15**(3), 487-495. https://doi.org/10.1007/s12205-011-0835-3.

Zhou, L. and Liu, Z. (2016), "Transverse bursting stresses due to horizontally curved tendons in the top slab of box girders", *J. Bridge Eng.*, **21**(2), 1-10. https://doi.org/10.1061/(ASCE)BE.1943-5592.0000863.

Zhou, L.Y., Liu, Z. and He, Z.Q. (2015), "Further investigation of transverse stresses and bursting forces in post-tensioned anchorage zones", *Struct. Concrete*, **16**(1), 84-92. https://doi.org/10.1002/suco.201400005.

CC